



HAL
open science

Sonoporation at a low mechanical index

Anthony Delalande, Spiros Kotopoulos, Tijs Rovers, Chantal Pichon, Michiel Postema

► **To cite this version:**

Anthony Delalande, Spiros Kotopoulos, Tijs Rovers, Chantal Pichon, Michiel Postema. Sonoporation at a low mechanical index. Bubble Science, Engineering & Technology, 2011, 3 (1), pp.3-12. hal-03186064

HAL Id: hal-03186064

<https://hal.science/hal-03186064v1>

Submitted on 30 Mar 2021

HAL is a multi-disciplinary open access archive for the deposit and dissemination of scientific research documents, whether they are published or not. The documents may come from teaching and research institutions in France or abroad, or from public or private research centers.

L'archive ouverte pluridisciplinaire **HAL**, est destinée au dépôt et à la diffusion de documents scientifiques de niveau recherche, publiés ou non, émanant des établissements d'enseignement et de recherche français ou étrangers, des laboratoires publics ou privés.

1 **Sonoporation at a low mechanical index**

2 Anthony Delalande

3 *Centre de Biophysique Moléculaire, UPR 4301 CNRS affiliated to the University of*
4 *Orléans, rue Charles Sadron, 45071 Orléans Cedex 2, France*

5 *e-mail: anthony.delalande@cnrs-orleans.fr*

6

7 Spiros Kotopoulos

8 *Department of Engineering, The University of Hull, Cottingham Road, Kingston upon*
9 *Hull HU6 7RX, United Kingdom*

10 *e-mail: Spiros.Kotopoulos@googlemail.com*

11

12 Tijs Rovers

13 *Emmy Noether Research Group, Institute of Medical Engineering, Department of*
14 *Electrical Engineering and Information Sciences, Ruhr-Universität Bochum, ID 04/24,*
15 *44780 Bochum, Germany*

16 *e-mail: Tijs.Rovers@rub.de*

17

18 Chantal Pichon

19 *Centre de Biophysique Moléculaire, UPR 4301 CNRS affiliated to the University of*
20 *Orléans, rue Charles Sadron, 45071 Orléans Cedex 2, France*

21 *e-mail: pichon@cnrs-orleans.fr*

22

23 Michiel Postema*

24 *Department of physics and technology, University of Bergen, Allégaten 55, 5007 Bergen,*
25 *Norway*

26 *and Emmy Noether Research Group, Institute of Medical Engineering, Department of*
27 *Electrical Engineering and Information Sciences, Ruhr-Universität Bochum, ID 04/24,*
28 *44780 Bochum, Germany*

29 *and Department of Engineering, The University of Hull, Cottingham Road,*
30 *Kingston upon Hull HU6 7RX, United Kingdom*

31 *and Centre de Biophysique Moléculaire, UPR 4301 CNRS affiliated to the University of*
32 *Orléans, rue Charles Sadron, 45071 Orléans Cedex 2, France*

33 *e-mail: michiel.postema@ift.uib.no*

34

35 *Corresponding author, e-mail michiel.postema@ift.uib.no

36 Running title: Sonoporation at a low mechanical index

37 Keywords: Sonoporation, Low mechanical index, Microbubbles, Ultrasound contrast
38 agent, HeLa cells, Cell penetration

39 **Abstract**

40 Purpose: The purpose of this study was to investigate the physical mechanisms of
41 sonoporation, in order to understand and improve ultrasound-assisted drug and gene
42 delivery. Sonoporation is the transient permeabilisation and resealing of a cell membrane
43 with the help of ultrasound and/or an ultrasound contrast agent, allowing for the
44 trans-membrane delivery and cellular uptake of macromolecules between 10 kDa and
45 3 MDa.

46 Methods: We studied the behaviour of ultrasound contrast agent microbubbles near
47 cancer cells at low acoustic amplitudes. After administering an ultrasound contrast
48 agent, HeLa cells were subjected to 6.6-MHz ultrasound with a mechanical index of 0.2
49 and observed with a high-speed camera.

50 Results: Microbubbles were seen to enter cells and rapidly dissolve. The quick
51 dissolution after entering suggests that the microbubbles lose (part of) their shell whilst
52 entering.

53 Conclusions: We have demonstrated that lipid-shelled microbubbles can be forced
54 to enter cells at a low mechanical index. Hence, if a therapeutic agent is added to the
55 shell of the bubble or inside the bubble, ultrasound-guided delivery could be facilitated
56 at diagnostic settings. In addition, these results may have implications for the safety
57 regulations on the use of ultrasound contrast agents for diagnostic imaging.

58 Introduction

59 Sonoporation is the transient permeabilisation and resealing of a cell membrane
60 with the help of ultrasound and/or an ultrasound contrast agent, allowing for the
61 trans-membrane delivery and cellular uptake of macromolecules between 10 kDa and
62 3 MDa.¹ Many studies have demonstrated increased drug and gene uptake of sites
63 under sonication.²⁻⁹ These studies presumed, that a physical membrane disruption
64 mechanism, *i.e.*, sonoporation, caused the increased uptake, as opposed to naturally
65 occurring active uptake processes, such as endocytosis, that are controlled by the
66 system biology.²⁻⁹ Although mechanical disruption with the aid of ultrasound has been
67 attributed to violent side effects of inertial cavitation and microbubble fragmentation,
68 most notably, the increased uptake has also been observed at low acoustic amplitudes,
69 *i.e.*, in acoustic regimes where inertial cavitation and microbubble fragmentation are not
70 to be expected. An ultrasound contrast agent microbubble might act as a vehicle to carry
71 a drug or gene load to a perfused region of interest. If the same ultrasound field that has
72 been implicated in the sonoporation process can cause release of the therapeutic load,
73 this load could be delivered into cells. Apart from plainly mixing ultrasound contrast
74 agents with therapeutic agents, several schemes have been proposed to incorporate
75 therapeutic loads to microbubbles. These include loads to the microbubble shell,¹⁰
76 therapeutic gases inside the microbubble,¹¹ gas-filled lipospheres containing drugs,¹²
77 and drug-filled antibubbles.¹³ To understand and ameliorate ultrasound-assisted drug
78 and gene delivery, the physics of controlled release and of sonoporation have been under
79 investigation. That objective also forms the focus for this paper. Moreover, we studied
80 the behaviour of ultrasound contrast agent microbubbles near cancer cells deliberately
81 at low acoustic amplitudes in order to probe whether sonoporation in this regime
82 was possible; and if so, to ascertain what the microscopic mechanism might entail; and
83 finally, to assess and scrutinise the safety aspects of ultrasound exposure in this regime.

84 Mechanical index

85 The mechanical index (MI) gives an indication of mechanical damage of tissue due to
86 inertial cavitation. It is defined by:

$$\text{MI} = \frac{p^-}{\sqrt{f_c}}, \quad (1)$$

87 where p^- is the maximum value of peak negative pressure anywhere in the ultrasound
88 field, measured in water but reduced by an attenuation factor equal to that which would
89 be produced by a medium having an attenuation coefficient of $0.3 \text{ dB cm}^{-1} \text{ MHz}^{-1}$,
90 normalised by 1 MPa, and f_c is the centre frequency of the ultrasound normalised by
91 1 MHz. For $\text{MI} < 0.3$, the acoustic amplitude is considered low. For $0.3 > \text{MI} > 0.7$, there
92 is a possibility of minor damage to neonatal lung or intestine.¹⁴ These are considered
93 moderate acoustic amplitudes. For $\text{MI} > 0.7$, there is a risk of cavitation if an ultrasound

94 contrast agent containing gas microspheres is being used, and there is a theoretical risk
95 of cavitation without the presence of ultrasound contrast agents.¹⁵ The risk increases
96 with MI values above this threshold. These are considered high acoustic amplitudes.
97 On commercial scanners, the MI has been limited to 1.9 for medical imaging.¹⁶ At low
98 MI, microbubbles pulsate linearly, whereas at high MI, their greater expansion phase
99 is followed by a violent collapse. During the collapse phase, when the kinetic energy
100 of the bubble surpasses its surface energy, a bubble may fragment into a number of
101 smaller bubbles. Fragmentation has been exclusively observed with contrast agents
102 with thin, elastic shells. Fragmentation is the dominant disruption mechanism for
103 these bubbles.¹⁷ Although the fragmentation of therapeutic load-bearing microbubbles
104 must release their loads, the actual drug or gene delivery is in this case a passive
105 process, dependent on diffusion rate and proximity to the target cells. Fragmenting
106 microbubbles may not create pores in cells, since fragmentation costs energy. However,
107 if a microbubble collapses near a free or a solid boundary, the retardation of the liquid
108 near the boundary may cause an asymmetry. This asymmetry causes differences in
109 acceleration on the bubble surface. During further collapse, a funnel-shaped jet may
110 protrude through the microbubble, shooting liquid to the boundary.¹⁸ The pore size
111 created by a jet has been empirically related to the microbubble expansion.¹⁹ If
112 jets could be directed to cell layers, in case of a microbubble carrying a therapeutic
113 load, the load could be delivered into cells. The jet formation is effected by the
114 cavitation topology, synergistically interacting with local fluid dynamics arising through
115 the bubble's expansion and contraction due to the ultrasound field. However, as the
116 fluid forming the microjet is just the bulk fluid which carries no therapeutic agent, then
117 there is no guarantee that, even with the formation of a sonopore due to jet impact with
118 the cell membrane, therapeutic agent will enter the cell. It needs to be dislodged and
119 mobilised from the bubble first. Furthermore, jetting has not been observed at low or
120 moderate MI,²⁰ so that fragmentation is likely to occur before any delivery takes place.
121 By pushing the loaded microbubbles towards the vessel wall using primary radiation
122 forces,²¹ release can take place closer to target vessels. In a recent study, Caskey *et*
123 *al.* pushed bubbles into tissue-mimicking gels at MI=1.5.²² We previously studied
124 how microclusters consisting of lipid-encapsulated microbubbles can be formed using
125 primary and secondary radiation forces, and how these clusters can be pushed towards
126 vessel walls.²³ We found that, even at MI<0.15, microbubble clusters can be formed
127 and pushed within seconds.

128 **Sonoporation**

129 There are five non-exclusive hypotheses for explaining the sonoporation phenomenon.
130 These have been summarised in Figure 1: push, pull, jetting, shear, and translation.²⁴
131 It has been hypothesised that expanding microbubbles might push the cell membrane
132 inward, and that collapsing bubbles might pull cell membranes outward.²⁵ These

133 mechanisms require microbubbles to be present in the close vicinity of cells. A separate
134 release mechanism should then ensure localised delivery. Although jetting only occurs
135 in a high-MI regime, it is very effective in puncturing cell membranes. Jetting has
136 been observed through cells using ultrasound contrast agent microbubbles. However,
137 the acoustic impedance of the solid cell substratum formed the boundary to which
138 the jetting took place, not the cell itself.²⁶ Also, there has not been any proof yet
139 of cell survival after jetting. In a separate study, we excluded the role of jetting as
140 a dominant mechanism in sonoporation.²⁷ If a microbubble is fixed to a membrane,
141 the fluid streaming around the oscillating bubbles creates enough shear to rupture the
142 membrane.²⁸ Here again, separate release mechanism should then ensure localised
143 delivery. Finally, it has been speculated that lipid-encapsulated microbubbles, in
144 compressed phase, translate through cell membranes or channels in the cell membrane.
145 In case of therapeutic loading, the load would be delivered directly into the target cell.
146 The main advantage of the latter mechanism is that microbubble translation by means
147 of ultrasonic radiation forces requires very low acoustic pressures. Hence, and potential
148 damaging bioeffects due to inertial cavitation can be ruled out.

149 **Materials and methods**

150 **Sonoporation configuration**

151 In previous studies, increased gene uptake was demonstrated at $MI < 0.3$.^{29,30} We
152 used a similar sonoporation configuration for our experiments. An overview of the
153 experimental setup is shown in Figure 2. A signal consisting of 50 cycles with a centre
154 frequency of 6.6 MHz and a pulse repetition frequency of 10 kHz, *i.e.*, a duty cycle
155 of 7.5%, was generated by an AFG 3102, dual channel arbitrary function generator
156 (Tektronix, Inc., Beaverton, OR, USA), amplified by a 150A250 radio-frequency (RF)
157 amplifier (Amplifier Research, Souderton, PA, USA) set to maximum gain, and fed
158 to a custom-built 6.6-MHz ultrasound transducer with a hexagonal lithium niobate
159 y -36°-cut active element with a maximum width of 25 mm.³¹ The peak-negative acoustic
160 pressure was measured to be 0.5 MPa in a separate tank and in the sonication chamber
161 itself. This corresponds to an MI of 0.2. The transducer was placed in a custom-built,
162 $260 \times 160 \times 150$ (mm)³ Perspex sonication chamber, in which an OptiCell[®] cell culture
163 chamber (Nunc GmbH & Co. KG, Langenselbold, Germany) was placed. One side of the
164 cell culture chamber contained a monolayer of 1.6×10^6 HeLa cells that had been cultured
165 in MEM with Earl's salts medium (PAA Laboratories GmbH, Pasching, Austria)
166 supplemented with 10% v/v heat-inactivated fetal calf serum, GlutaMAX[™] (Life
167 Technologies Gibco, Paisley, Renfrewshire, UK), 1% v/v of non-essential amino-acids
168 (PAA), penicillin ($100 \text{ units ml}^{-1}$) and streptomycin ($100 \mu\text{g ml}^{-1}$) (PAA), at 37°C in
169 a humidified atmosphere containing 5% CO₂. The cells were used when there was
170 60–80% confluency. Ultrasound contrast agent was injected into the cell culturing

171 chamber before each experiment. Several lipid-shelled ultrasound contrast agents
172 were tested in this study. In this paper, we present results of a 3.33% dilution of
173 MicroMarkerTM (VisualSonics B.V., Amsterdam, Netherlands), a lipid-shelled agent
174 with a mean diameter of 2.5 μm . A customised BXFM-F microscope unit with an
175 LCach N 20 \times /0.40 PhC (Olympus Deutschland GmbH, Hamburg, Germany) and a
176 LUMPlanFL 60 \times /0.90 water-immersion objective (Olympus) was placed on top of the
177 sonication chamber. The colour charge coupled device (CCD) of a PHOTRON FastCam
178 MC-2.1 high-speed camera (VKT Video Kommunikation GmbH, Pfullingen, Germany)
179 was connected to the microscope. The sensor was rotated to make sure that in all
180 recorded movies, the ultrasound is directed from the left to the right of the frame.

181 Fluorescence configuration

182 An overview of the setup used for the fluorescence experiments is shown in Figure 3.
183 It is almost identical to the setup described in the previous section. However, here,
184 the signal consisting of 40 cycles with a centre frequency of 6.6 MHz and a pulse
185 repetition frequency of 10 kHz, *i.e.*, a duty cycle of 6.1%, was amplified using a 2100L,
186 +50-dB RF amplifier (Electronics & Innovation, Rochester, NY, USA) and fed to our
187 custom-built 6.6-MHz ultrasound transducer.³¹ Prior to injection in the OptiCell[®], the
188 MicroMarker[®] contrast agent was labelled using a DiD (DiI_{C18}(5)) lipophilic fluorescent
189 probe (VybrantTM Molecular probes, Invitrogen, San Diego, CA, USA). A ratio of 1 μl of
190 DiD to 40 μl MicroMarker[®] was homogenised by pipetting and incubating for 5 minutes
191 at room temperature. Figure 4 shows how the DiD fluorescent probe bonded to the
192 phospholipid.³² Emitted $\lambda=649\text{--}703$ nm fluorescence was localised on the microbubble
193 shell when exciting at $\lambda=633$ nm. A custom-made aluminium sonication chamber with
194 internal dimensions of 130 \times 170 \times 35 (mm)³ was locked into to the xy -stage of a 200M
195 inverted confocal microscope (Carl Zeiss AG, Oberkochen, Germany) coupled with a
196 LSM Axiovert 510 scanning device (Carl Zeiss), using an EC Plan-Neofluar 40 \times /1.30
197 Oil DIC M27 objective (Carl Zeiss AG), with automated z -stack functionality.

198 The peak-negative acoustic pressure was measured at the objective's field of view
199 and corresponded to MI =0.2.

200 To ensure that the microbubbles were not naturally attracted to the cells,
201 30 μl MicroMarker[®] was diluted into 700 μl of distilled water and tested for
202 electrophoretic mobility (ζ -potential) using a Zetasizer 3000 (Malvern Instruments,
203 Malvern, Worcestershire, United Kingdom).

204 To measure the thickness of the cultured cells 10⁵ HeLa cells were seeded into a
205 OptiCell[®]. The cell plasma membrane was labelled with DiD lipophilic fluorescent
206 probe (VybrantTM Molecular probes) according to the manufacturers protocol. The
207 membrane fluorescence was measured using a 200M confocal microscope. Cell thickness
208 was calculated from the difference between the upper and lower slices where fluorescence
209 was seen.

210 We recorded 23 movies under 6.6-MHz sonication at frame rates between 500 and
211 2000 frames per second, representing 15 minutes of real-time exposure. Of these, 11
212 movies were recorded using fluorescence. In addition we recorded 10 control movies,
213 with a total duration of 22 minutes.

214 Results and discussion

215 Throughout this section, the optical z -axis is defined from distal-to-focus (negative) to
216 proximal-to-focus (positive), with $z = 0$ as the focal plane.

217 Figure 5 shows z -stacks of fluorescence emitted by the DiD dye attached to the
218 membranes of four typical HeLa cells, representing the cell geometry. In total, the
219 thicknesses of 42 cells were measured. The cultured cells were found to be $13 \pm 2 \mu\text{m}$
220 thick. Clearly, these cells had thicknesses much greater than ultrasound contrast agent
221 microbubble oscillations amplitudes at $\text{MI}=0.2$.

222 We analysed our optical system and compared our results to bubbles and cells that
223 were slightly out of focus, to rule out that the movement of the bubble takes place in a
224 plane different from that of the cell. Figure 6 shows a z -stack of two ultrasound contrast
225 agent microbubbles, similar to Figure 10 of Postema *et al.*³³ Proximal-to-focus Airy
226 disks can be seen around the bubbles, whereas distal-to-focus the bubble boundaries are
227 blurred. Note that the boundary contrast is maximal just proximal-to-focus.³³

228 At a centre frequency of 6.6 MHz, we recorded 17 events of microbubbles entering
229 HeLa cells. After entering, the microbubbles were observed to quickly dissolve. As an
230 example, Figure 7 shows an event resampled at 3.4 Hz and 40 Hz, respectively, where
231 two bubbles were pushed to a cell during 11 s of sonication. A microbubble “A” of $4\text{-}\mu\text{m}$
232 diameter entered the cell and dissolved, whereas a microbubble “B” of $2\text{-}\mu\text{m}$ diameter
233 stuck to the cell membrane.

234 Figures 8 and 9 show two similar events, where fluorescence-coated microbubbles
235 were used. The left panels show a microbubble apparently penetrating through the cell
236 membrane in optical focus. Approximately 70 ms after the ultrasound has been switched
237 on a microbubble is seen to penetrate through the cell membrane in Figure 8. In Figure 9
238 the microbubble is seen to penetrate through the cell membrane approximately 24 ms
239 after the ultrasound has been switched on. The right panels show a z -stack through the
240 entire cell, to record whether the apparent microbubble entry is actually into the cell.

241 For both events, Figure 10 shows average fluorescent intensities in two regions of
242 interest, one inside the cell, and one control region. In both events, most fluorescence
243 from apparent microbubble entry can be observed within $5 \mu\text{m}$ proximal to optical focus,
244 thus well within the cells themselves.

245 Figure 11 shows frames in optical focus from the events in Figures 8 and 9, before
246 sonication and approximately 8 minutes after sonication. Clearly, fluorescence has
247 transferred into the cells and remained inside the cells long after sonication.

248 At these low acoustic amplitudes, inertial cavitation, fragmentation, and jetting
249 should not occur. Hence, as a mechanism in sonoporation at low MI, these phenomena
250 might justifiably be neglected.

251 Our observations do not explain why some microbubbles enter a cell and others
252 don't. The quick dissolution after entering suggests that the microbubble loses (part of)
253 its shell whilst entering.

254 The ζ -potential measurements showed that the microbubble shells had a charge of
255 -43.9 ± 2.4 mV. As cells have a natural negative charge,^{34,35} the ultrasound contrast
256 agent should be repelled by the cells, in our recordings we see that, once the ultrasound
257 was turned on, the microbubbles would be attracted to the closest cell, independent of
258 the direction of the sound field. This supports the recent finding that cell membranes
259 can be acoustically active,³⁶ and therefore interact with microbubbles.

260 Other cell types than HeLa cells must be used in follow-up studies, to investigate
261 differences in bubble–cell interaction.

262 Conclusions

263 We have demonstrated that lipid-shelled microbubbles can be forced to enter cells at a
264 low MI. Hence, if a therapeutic load is added to the bubble, ultrasound-guided delivery
265 could be facilitated at diagnostic settings.

266 In addition, these results may have implications for the safety regulations on the use
267 of ultrasound contrast agents for diagnostic imaging.

268 Acknowledgements

269 This work has been supported by DFG Emmy Noether Programme Grant 38355133
270 and EPSRC Grant EP/F037025/1. The authors are grateful to Conseil Regional for
271 A. Delalande's fellowship.

272 References

- 273 ¹ M. Postema and O. H. Gilja, *Curr. Pharm. Biotechnol.*, 2007, **8(6)**, 355–361.
- 274 ² S. Bao, B. D. Thrall and D. L. Miller, *Ultrasound Med. Biol.*, 1997, **23**, 953–959.
- 275 ³ S. Chen, R. V. Shohet, R. Bekeridjian, P. Frenkel and P. A. Grayburn, *J. Am. Coll.*
276 *Cardiol.*, 2003, **42(2)**, 301–308.
- 277 ⁴ W. J. Greenleaf, M. E. Bolander, G. Sarkar, M. B. Goldring and J. F. Greenleaf,
278 *Ultrasound Med. Biol.*, 1998, **24(4)**, 587–595.

- 279 ⁵ I. Kondo, K. Ohmori, A. Oshita, H. Takeuchi, S. Fuke, K. Shinomiya, T. Noma,
280 T. Namba and M. Kohno, *J. Am. Coll. Cardiol.*, 2004, **44(3)**, 644–653.
- 281 ⁶ N. Kudo, K. Okada and K. Yamamoto, *Biophys. J.*, 2006, **96(12)**, 4866–4876.
- 282 ⁷ J. Lindner and S. Kaul, *Echocardiography*, 2001, **18(4)**, 329–337.
- 283 ⁸ K. Tachibana, T. Uchida, K. Ogawa, N. Yamashita and K. Tamura, *Lancet*, 1999,
284 **353**, 1409.
- 285 ⁹ S. Tinkov, R. Bekeredjian, G. Winter and C. Coester, *J. Pharm. Sci.*, 2009, **98(6)**,
286 1935–1961.
- 287 ¹⁰ A. L. Klibanov, *Adv. Drug Delivery Rev.*, 1999, **37**, 139–157.
- 288 ¹¹ M. Postema, A. Bouakaz, F. J. ten Cate, G. Schmitz, N. de Jong and A. van Wamel,
289 *Ultrasonics*, 2006, **44(S1)**, e109–e113.
- 290 ¹² M. J. Shortencarier, P. A. Dayton, S. H. Bloch, P. A. Schumann, T. O. Matsunaga
291 and K. W. Ferrara, *IEEE Trans. Ultrason., Ferroelect., Freq. Contr.*, 2004, **51(7)**,
292 822–831.
- 293 ¹³ M. Postema, F. J. ten Cate, G. Schmitz, N. de Jong and A. van Wamel, *Lett. Drug*
294 *Des. Discov.*, 2007, **4(1)**, 74–77.
- 295 ¹⁴ British Medical Ultrasound Society: ‘Guidelines for the safe use of diagnostic
296 ultrasound equipment’, 2000.
- 297 ¹⁵ G. ter Haar, *Med Biol Eng Comput*, 2009, **47**, 893–900.
- 298 ¹⁶ J.-U. Voigt, *Methods*, 2009, **48**, 92–97.
- 299 ¹⁷ M. Postema and G. Schmitz, *Ultrason. Sonochem.*, 2007, **14(4)**, 438–444.
- 300 ¹⁸ A. Philipp and W. Lauterborn, *J. Fluid Mech.*, 1998, **361**, 75–116.
- 301 ¹⁹ T. Kodama and K. Takayama, *Ultrasound Med. Biol.*, 1998, **24(5)**, 723–738.
- 302 ²⁰ M. Postema, A. van Wamel, F. J. ten Cate and N. de Jong, *Med. Phys.*, 2005, **32(12)**,
303 3707–3711.
- 304 ²¹ P. A. Dayton, J. S. Allen and K. W. Ferrara, *J. Acoust. Soc. Am.*, 2002, **112(5)**,
305 2183–2192.
- 306 ²² C. Caskey, S. Qin, P. A. Dayton and K. W. Ferrara, *J. Acoust. Soc. Am.*, 2009,
307 **125(5)**, EL183–EL189.
- 308 ²³ S. Kotopoulis and M. Postema, *Ultrasonics*, 2010, **50**, 260–268.

- 309 ²⁴ M. Postema, O. H. Gilja and A. van Wamel: ‘Fundamentals of Medical Ultrasonics’,
310 ed. M. Postema, Spon press, London, 2011, 205–217.
- 311 ²⁵ A. van Wamel, K. Kooiman, M. Harteveld, M. Emmer, F. J. ten Cate, M. Versluis
312 and N. de Jong, *J. Control. Release*, 2006, **112(2)**, 149–155.
- 313 ²⁶ P. Prentice, A. Cuschieri, K. Dholakia, M. Prausnitz and P. Campbell, *Nature Phys.*,
314 2005, **1**, 107–110.
- 315 ²⁷ M. Postema and O. H. Gilja, *Biomed. Eng.*, 2010, **55**, S19–S20.
- 316 ²⁸ P. Marmottant and S. Hilgenfeldt, *Nature*, 2003, **423**, 153–156.
- 317 ²⁹ A. Delalande, M.-F. Bureau, P. Midoux, A. Bouakaz and C. Pichon, *Ultrasonics*,
318 2009, **50**, 269–272.
- 319 ³⁰ K. Kaddur, L. Lebegue, F. Tranquart, P. Midoux, C. Pichon and A. Bouakaz, *IEEE*
320 *Trans. Ultrason. Ferroelectr. Freq. Control*, 2010, **57(7)**, 1558–1567.
- 321 ³¹ S. Kotopoulis, H. Wang, S. Cochran and M. Postema, *Proc. IEEE Ultrason. Symp.*,
322 2010, accepted.
- 323 ³² P. Livanec and R. Dunn, *Langmuir*, 2008, **24(24)**, 14066–14073.
- 324 ³³ M. Postema, A. Bouakaz, C. T. Chin and N. de Jong, *IEEE Trans. Ultrason.*,
325 *Ferroelectr., Freq. Control*, 2003, **50(5)**, 523–536.
- 326 ³⁴ B. Ehrenberg, V. Montana, M.-D. Wei, J. Wuskell and L. Loew, *Biophys. J.*, 1988,
327 **53**, 785–794.
- 328 ³⁵ A. Takahashi, H. Yamaguchi and H. Miyamoto, *Am. J. Physiol.*, 1993, **265(2)**,
329 C328–C336.
- 330 ³⁶ B. Krasovitski, V. Frenkel, S. Shoham and E. Kimmel, *Proc. Nat. Acad. Sci.*, 2011,
331 accepted.

332 **List of Figures**

333 1 Possible mechanisms of sonoporation: a) push, b) pull, c) jetting, d)
334 shear, e) translation. Based on Figure 9.2 in Postema *et al.*²⁴ 13

335 2 Experimental setup (*top*) and a close-up of the sonoporation configuration
336 (*bottom*). 14

337 3 Experimental setup (*top*) and a close-up of the fluorescence configuration
338 (*bottom*). 15

339 4 Schematic representation of DiD (DiI_{C18}(5)) lipophilic fluorescent probe
340 bonding to phospholipid.³² 16

341 5 *z*-stacks of fluorescence emitted by the DiD dye attached to the
342 membranes of four typical HeLa cells, representing the cell geometry. . . 17

343 6 *z*-stack of two ultrasound contrast agent microbubbles. Proximal-to-focus
344 Airy disks can be seen around the bubbles, whereas distal-to-focus the
345 bubble boundaries are blurred. Microbubble A has a diameter of 2 μm ,
346 whereas microbubble B has a diameter of 3 μm . Each frame corresponds
347 to a $11 \times 11 (\mu\text{m})^2$ area. 18

348 7 A sonoporation event including microbubble dissolution during 11s of
349 sonication (*left*) and selected frames of the microbubble entering a
350 cell (*right*). Microbubble “A” entered the cell and dissolved, whereas
351 microbubble “B” stuck to the cell membrane. Each frame corresponds to
352 a $23 \times 23 (\mu\text{m})^2$ area. 19

353 8 Microbubble of 5- μm diameter apparently penetrating through the cell
354 membrane in optical focus (*left*); *z*-stack through the entire cell, to record
355 whether the apparent microbubble entry is actually into the cell (*right*).
356 Areas (A) and (C) are regions of interest inside and outside the cell,
357 respectively. Each frame corresponds to a $76 \times 76 (\mu\text{m})^2$ area. 20

358 9 Microbubble of 4- μm diameter apparently penetrating through the cell
359 membrane in optical focus (*left*); *z*-stack through the entire cell, to record
360 whether the apparent microbubble entry is actually into the cell (*right*).
361 Areas (A) and (C) are regions of interest of high fluorescence and low
362 fluorescence, respectively, inside the cell. The white dotted lines in the
363 upper left frame of the right panel indicates the cell membrane. Each
364 frame corresponds to a $52 \times 52 (\mu\text{m})^2$ area. 21

365 10 Average fluorescent intensities in the regions of interest (ROI) of Figures 8
366 (*left*) and 9 (*right*). Bold lines represent ROI (A) inside the cells, whereas
367 hairlines represent ROI (C) the control regions. The dotted line represents
368 the cell boundary contrast. Note that the cell boundary contrast is
369 maximal just proximal-to-focus. 22

370 11 Columns (a) and (b) represent frames in optical focus from the events
371 in Figures 8 and 9, respectively, before sonication and approximately
372 8 minutes after sonication. The white dotted lines in the right frames
373 indicate the cell membrane boundary. The left frames correspond to
374 $76 \times 76 (\mu\text{m})^2$ areas, whereas the right frames correspond to $45 \times 45 (\mu\text{m})^2$
375 areas. 23

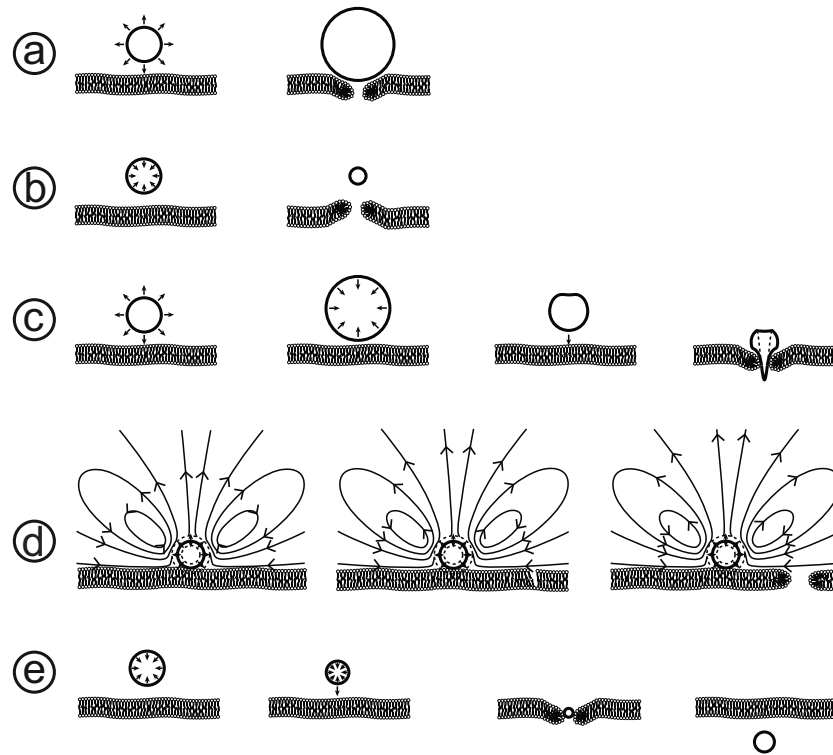


Figure 1: Possible mechanisms of sonoporation: a) push, b) pull, c) jetting, d) shear, e) translation. Based on Figure 9.2 in Postema *et al.*²⁴

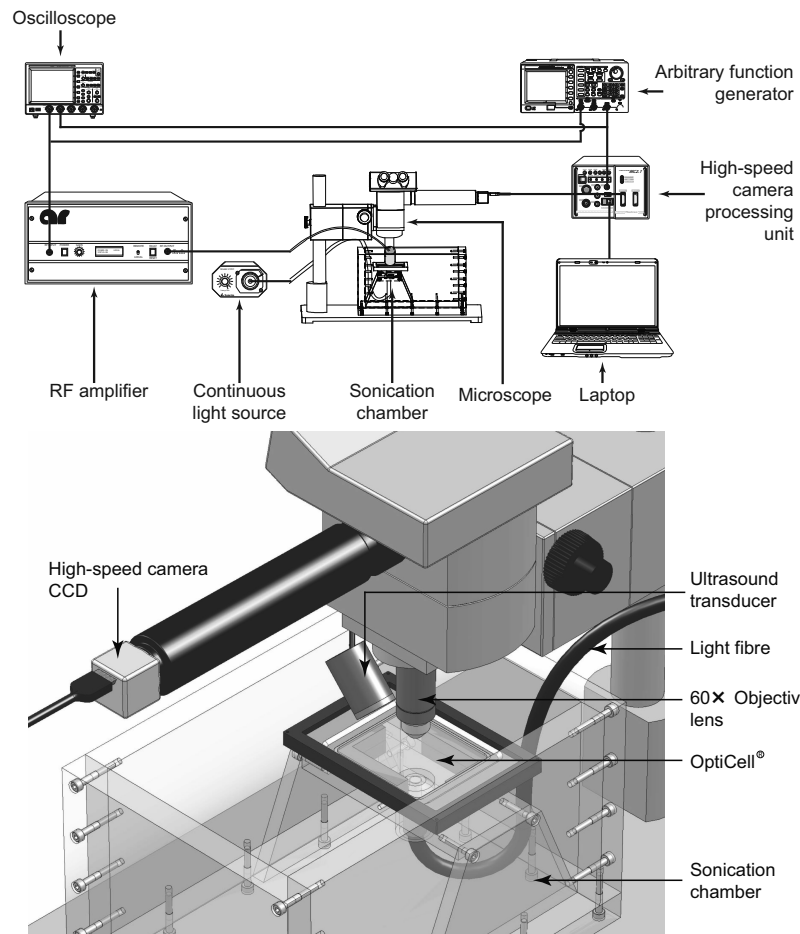


Figure 2: Experimental setup (*top*) and a close-up of the sonoporation configuration (*bottom*).

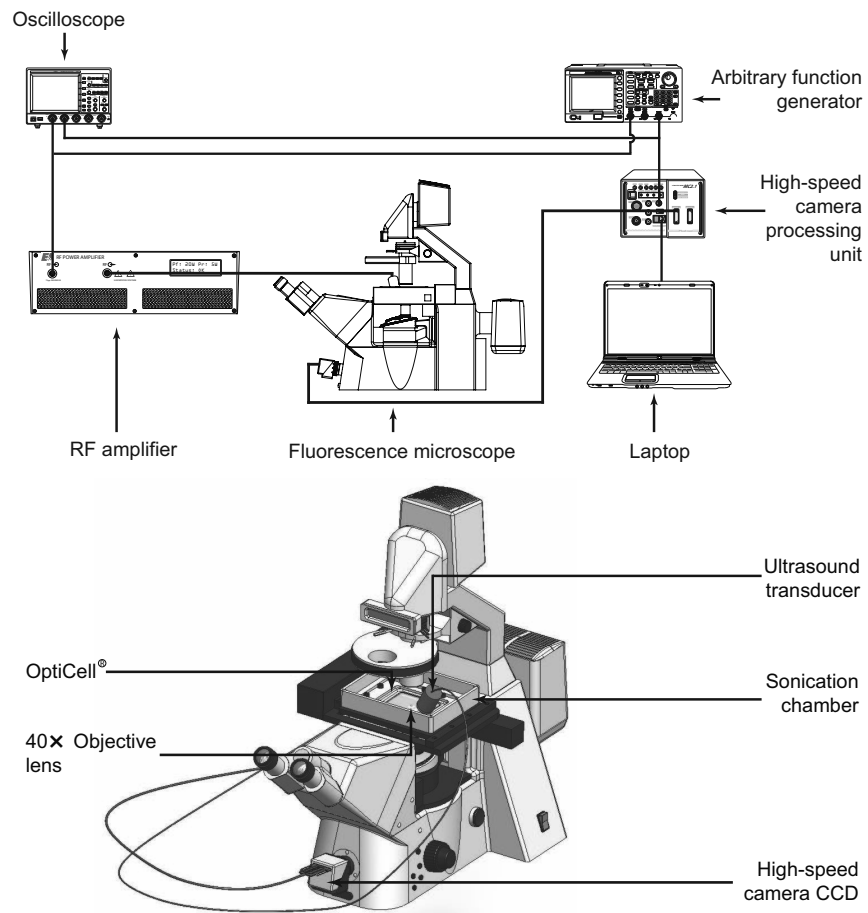


Figure 3: Experimental setup (*top*) and a close-up of the fluorescence configuration (*bottom*).

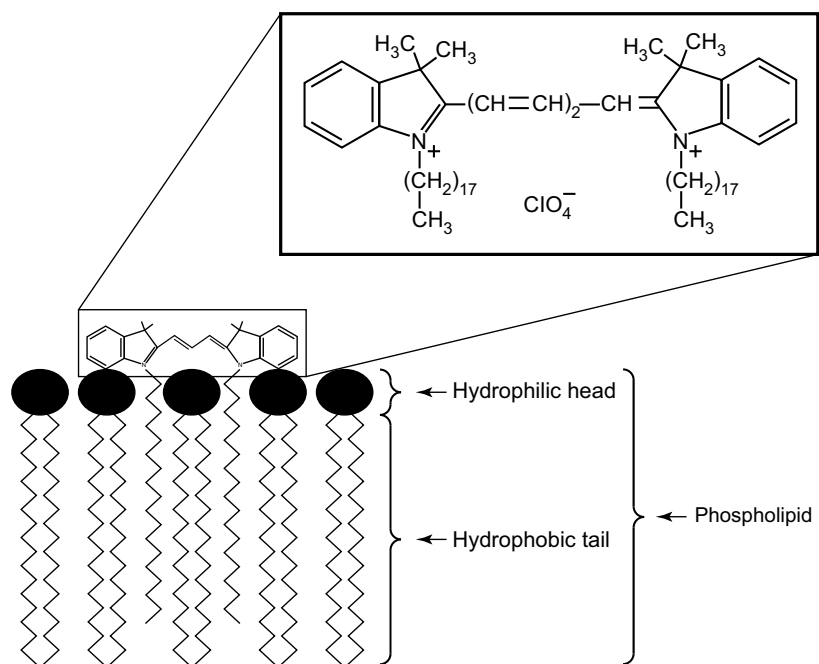


Figure 4: Schematic representation of DiD (DiI₁₈(5)) lipophilic fluorescent probe bonding to phospholipid.³²

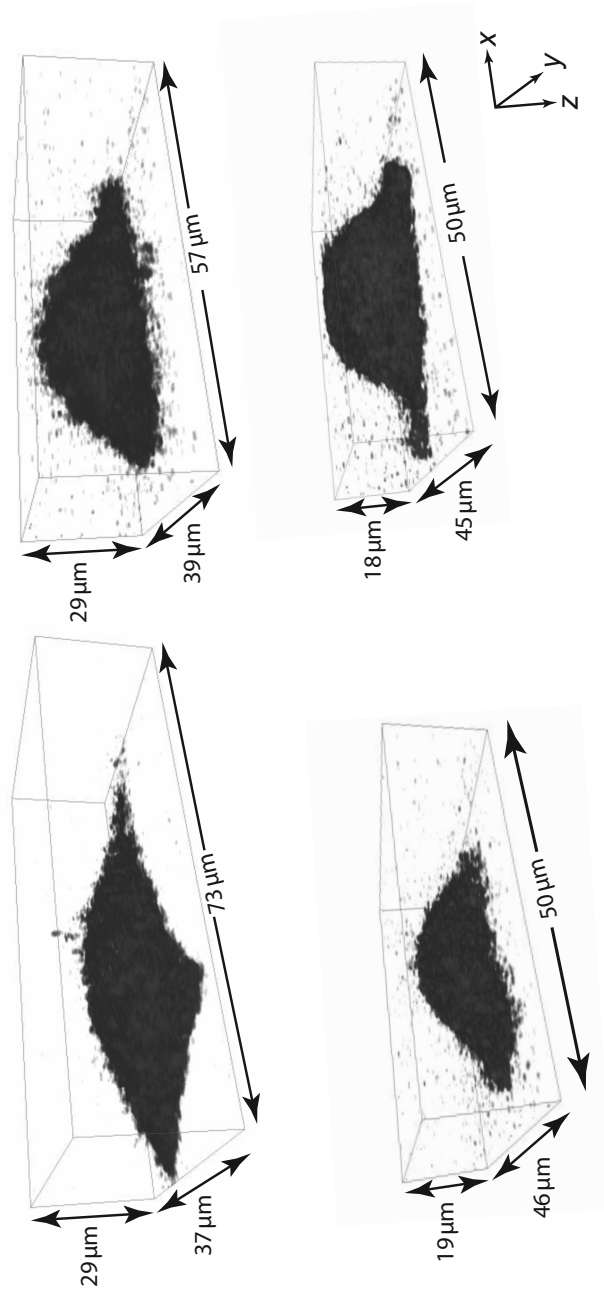


Figure 5: z -stacks of fluorescence emitted by the DiD dye attached to the membranes of four typical HeLa cells, representing the cell geometry.

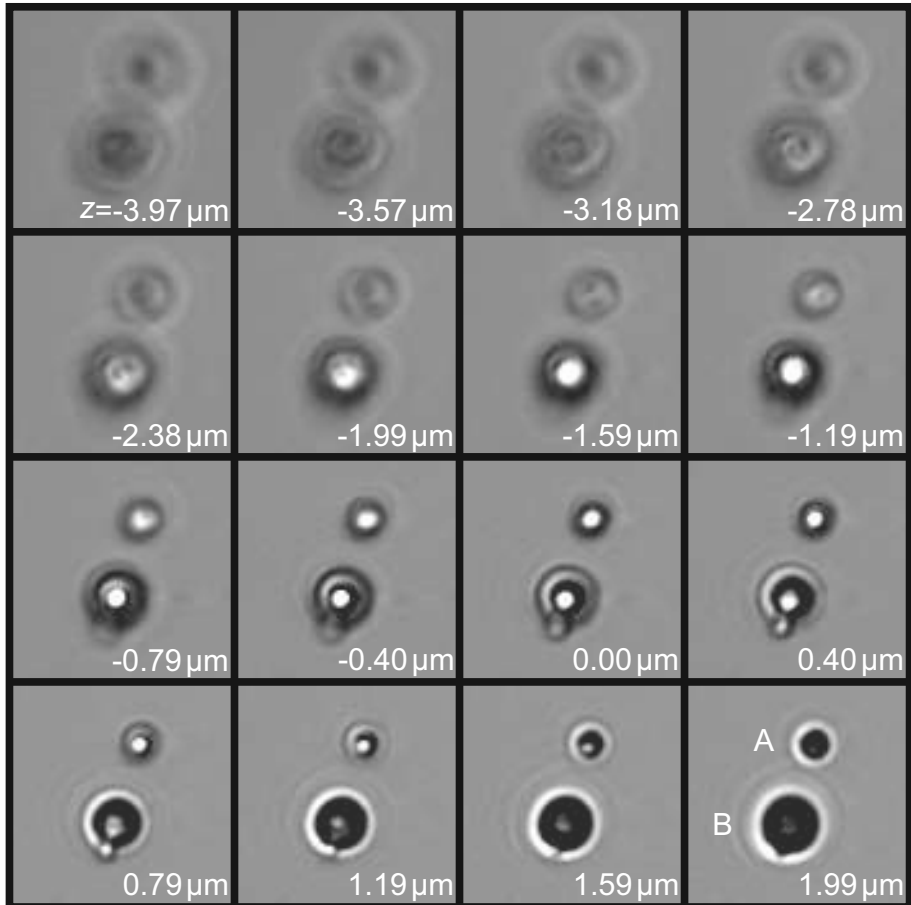


Figure 6: z -stack of two ultrasound contrast agent microbubbles. Proximal-to-focus Airy disks can be seen around the bubbles, whereas distal-to-focus the bubble boundaries are blurred. Microbubble A has a diameter of $2\ \mu\text{m}$, whereas microbubble B has a diameter of $3\ \mu\text{m}$. Each frame corresponds to a $11 \times 11\ (\mu\text{m})^2$ area.

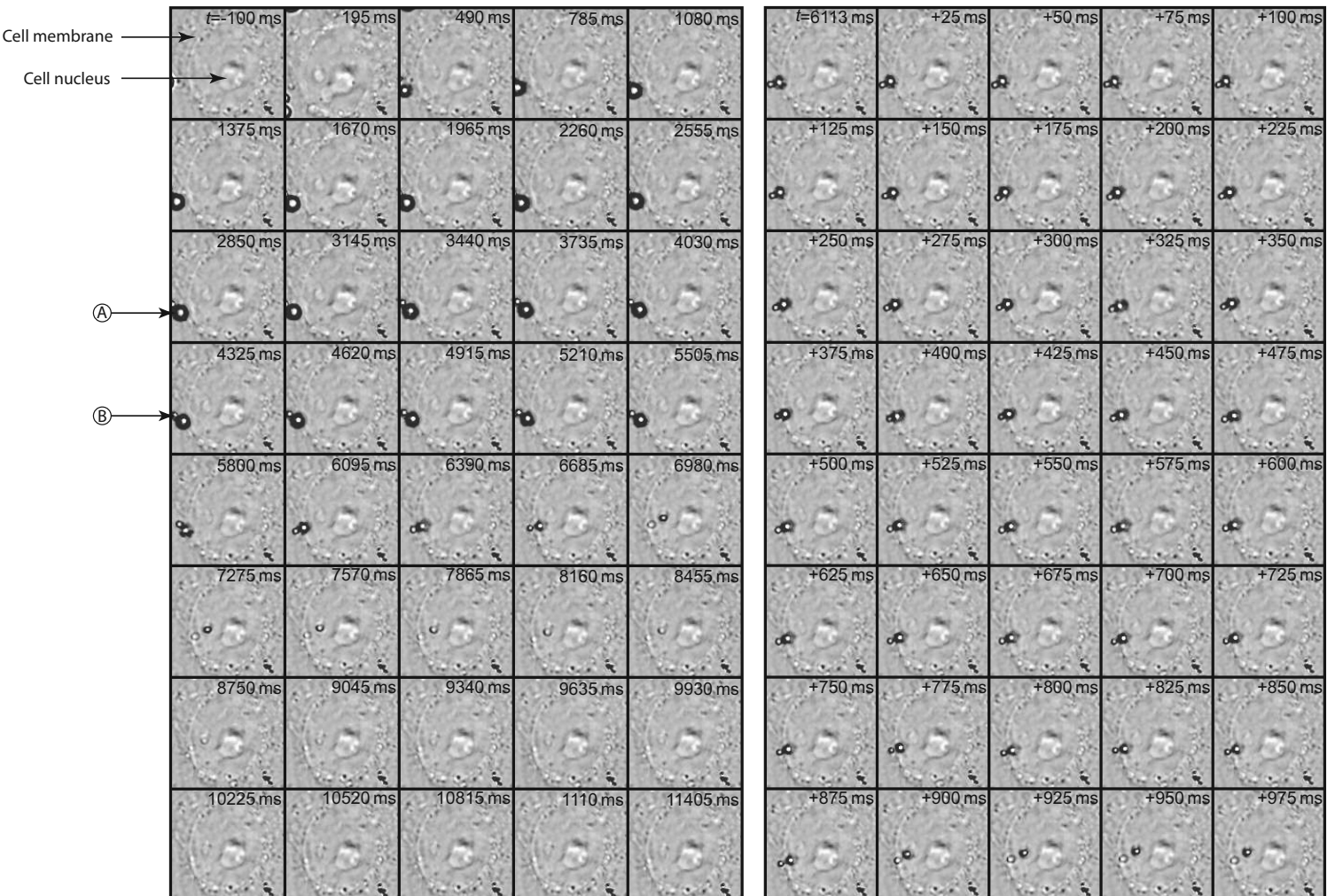


Figure 7: A sonoporation event including microbubble dissolution during 11 s of sonication (*left*) and selected frames of the microbubble entering a cell (*right*). Microbubble “A” entered the cell and dissolved, whereas microbubble “B” struck to the cell membrane. Each frame corresponds to a $23 \times 23 (\mu\text{m})^2$ area.

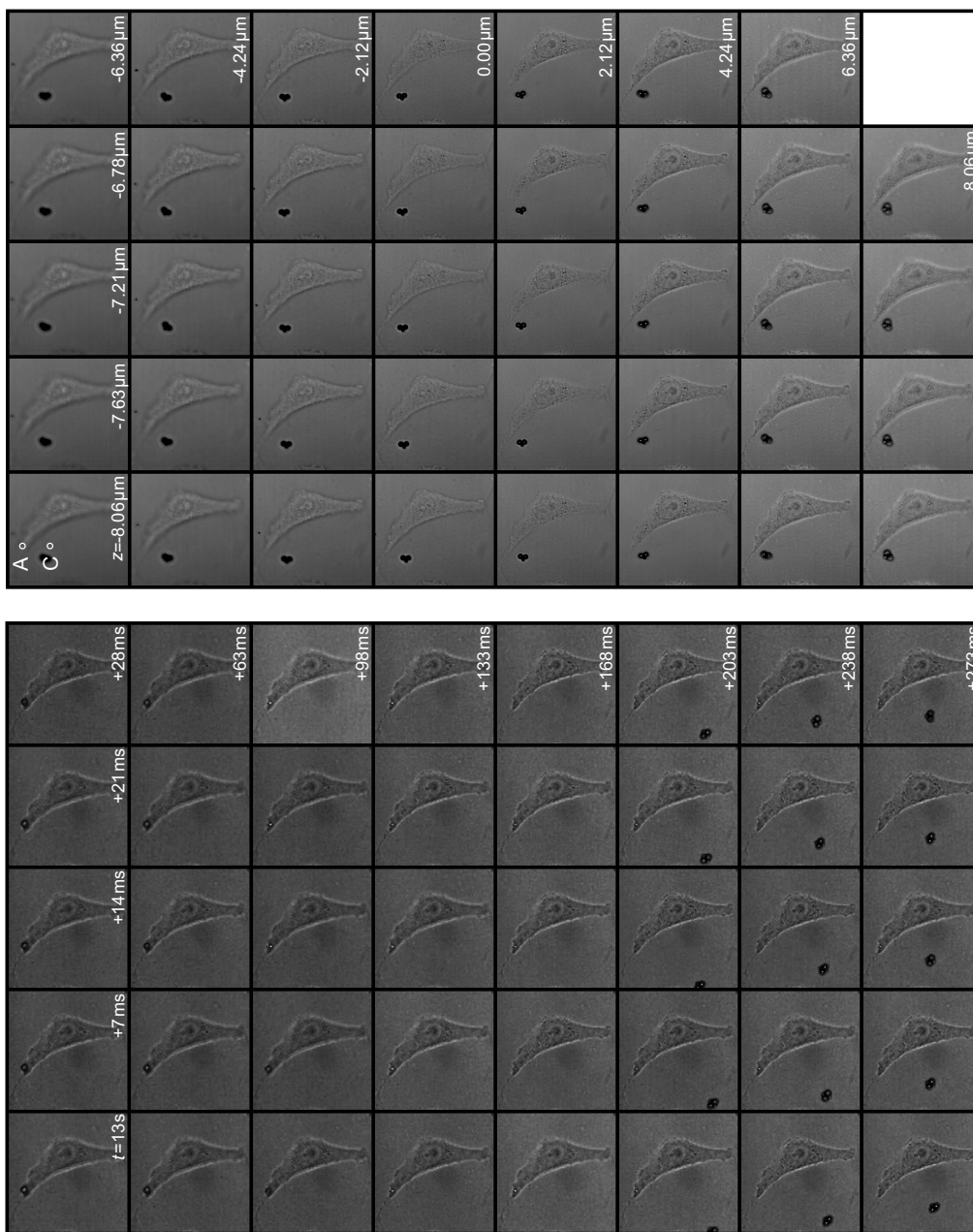


Figure 8: Microbubble of $5\text{-}\mu\text{m}$ diameter apparently penetrating through the cell membrane in optical focus (*left*); *z*-stack through the entire cell, to record whether the apparent microbubble entry is actually into the cell (*right*). Areas (A) and (C) are regions of interest inside and outside the cell, respectively. Each frame corresponds to a $76 \times 76 (\mu\text{m})^2$ area.

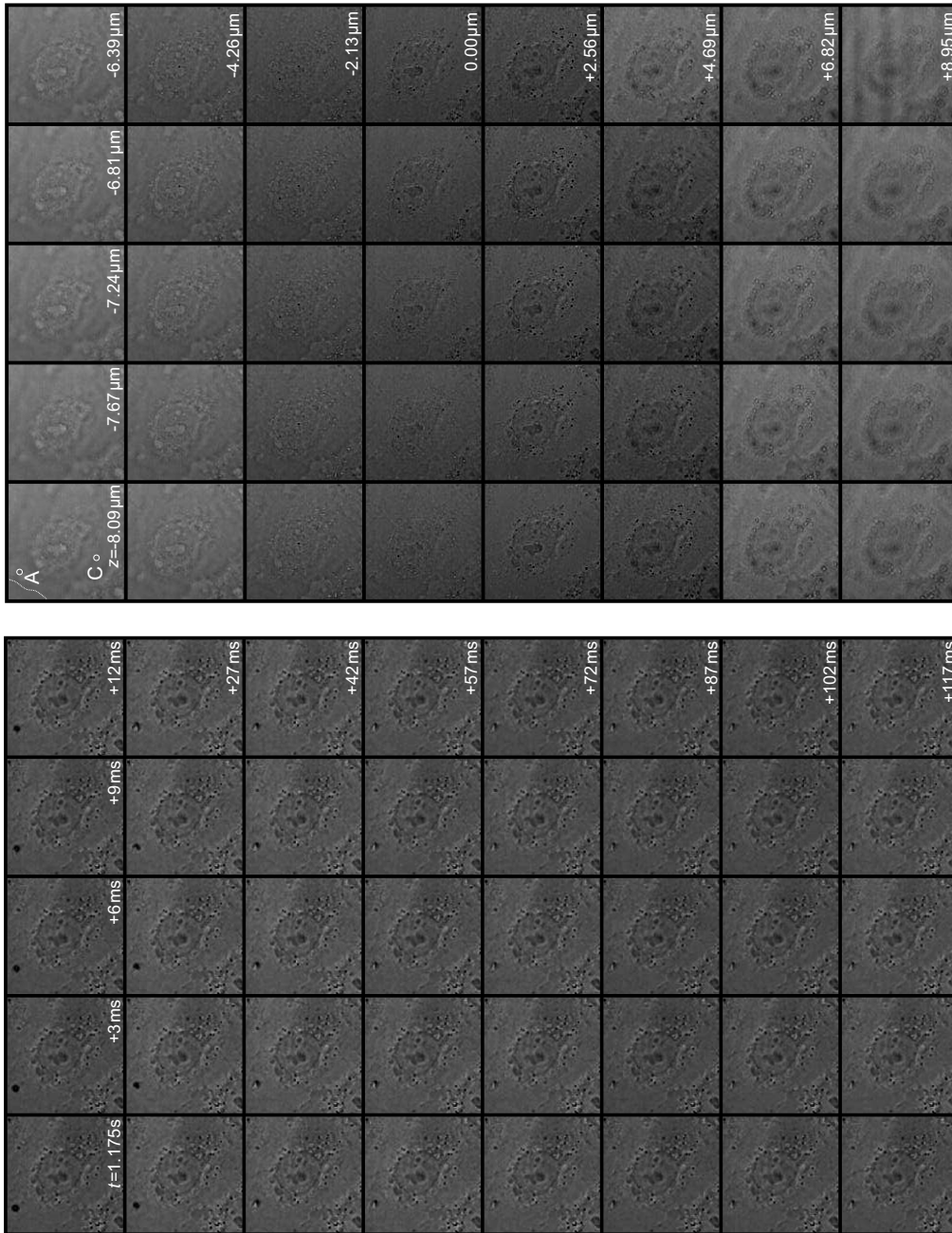


Figure 9: Microbubble of $4\text{-}\mu\text{m}$ diameter apparently penetrating through the cell membrane in optical focus (*left*); z -stack through the entire cell, to record whether the apparent microbubble entry is actually into the cell (*right*). Areas (A) and (C) are regions of interest of high fluorescence and low fluorescence, respectively, inside the cell. The white dotted lines in the upper left frame of the right panel indicates the cell membrane. Each frame corresponds to a $52 \times 52 (\mu\text{m})^2$ area.

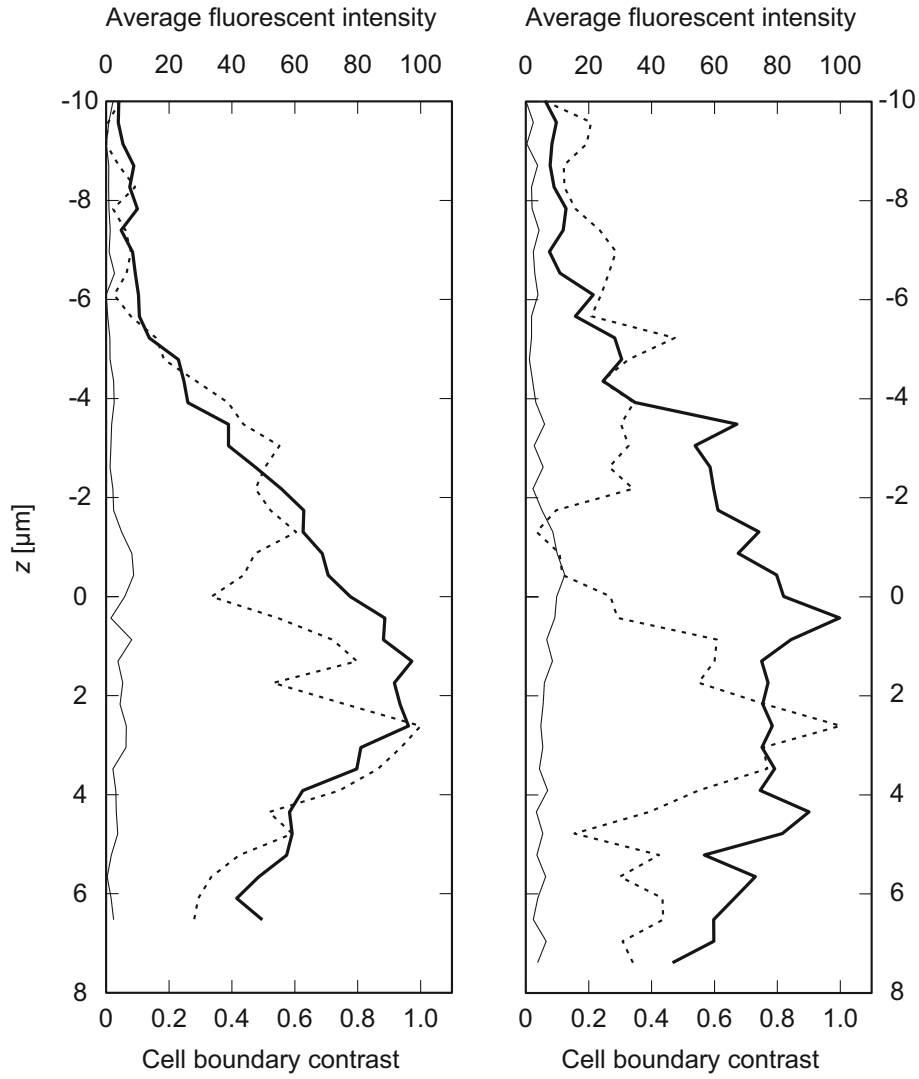


Figure 10: Average fluorescent intensities in the regions of interest (ROI) of Figures 8 (*left*) and 9 (*right*). Bold lines represent ROI (A) inside the cells, whereas hairlines represent ROI (C) the control regions. The dotted line represents the cell boundary contrast. Note that the cell boundary contrast is maximal just proximal-to-focus.

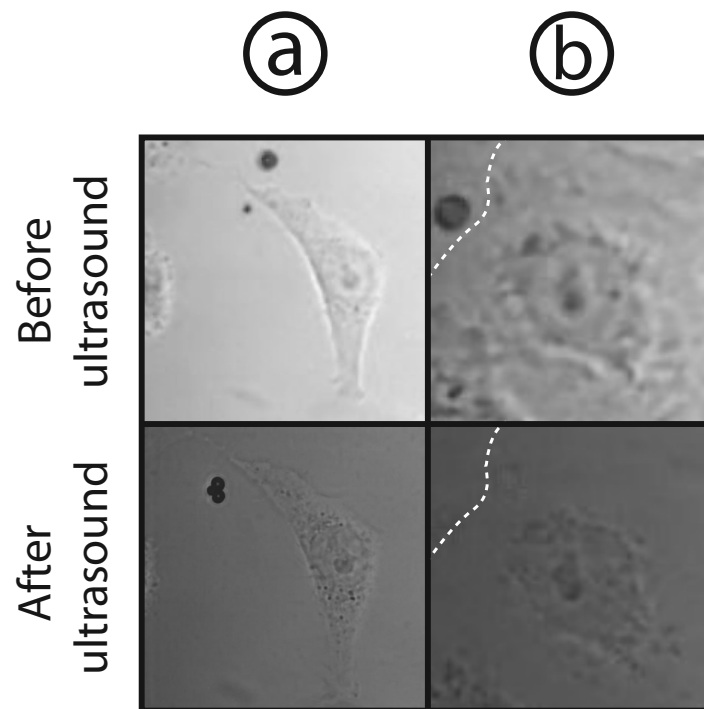


Figure 11: Columns (a) and (b) represent frames in optical focus from the events in Figures 8 and 9, respectively, before sonication and approximately 8 minutes after sonication. The white dotted lines in the right frames indicate the cell membrane boundary. The left frames correspond to $76 \times 76 (\mu\text{m})^2$ areas, whereas the right frames correspond to $45 \times 45 (\mu\text{m})^2$ areas.